Journal of
Renewable Energy Research and Applications (RERA)

*Vol. 6, No 1, 2024, 139-150* *DOI: 10.22044/rera.2024.13393.1235*

# Design and Multi-criteria Evaluation of a Hydrokinetic Turbine Rotor in Water Transfer Canals for Electricity Generation

O. Rasooli, M. Ebrahimi* and A. Babamiri

*Mechanical engineering department, University of Kurdistan, Sanandaj, Kurdistan, Iran.*

Received Date 19 July 2023; Revised Date 01 January 2024; Accepted Date 12 January 2024
**Corresponding author: ma.ebrahimi@uok.ac.ir (M. Ebrahimi)*

**Abstract**

In the present research work, a hydrokinetic turbine is designed, and evaluated technically, economically and environmentally, to produce power from low-velocity currents. Firstly, the hydraulic characteristics of three existing canals is investigated, and the blade profile for the turbine rotor is determined by using the Schmitz's theory and the XFOIL software. The geometrical model is then created in the SolidWorks, and simulated in the ANSYS Fluent to estimate the power generation capacity. According to the results, a correlation is proposed to estimate the power generation by the turbine in different water velocities. The results are validated with the manufacturers data. The results show that the efficiency of the proposed turbine is almost 90%, the investment payback period is only 3.1 years, with a positive net present value. Environmentally, it shows that for a 1 meter in diameter turbine and water velocity of 1.5 m/s, carbon dioxide will reduce by 0.57 tons per year. The economic and environmental benefits improve greatly at higher water velocities. The results show that the proposed hydrokinetic turbine even by working in low velocity stream can supply electricity demand of rural area near the canals for the long lifespan of the turbine, which is more than 25 years.

**Keywords:** *Hydrokinetic turbine, Canal, ANSYS Fluent, XFOIL, Schmitz's theory, Cavitation, Carbon saving, Payback period.*

## 1. Introduction

Climate change and global warming are among the top concerns of scientists, and they are continuously warning and advising people, governments, industrialists, environmental activists, etc. about the catastrophic impacts of greenhous gases (GHGs). The Net Zero Emission 2050 (NZE) scenario is the global agreement to avoid the GHG impacts and keep the temperature rise below 1.5 ℃ above the pre-industrial temperature. Until now, the temperature has increased by 1.1 ℃ compared to the 1800s. In order to prevent the increase in temperature by more than 1.5 ℃, the amount of pollutants should be reduced by 45% by 2030 and reach zero by 2050 (Paris Agreement) [1].

In order to adhere to the Paris Agreement and implement it according to the schedule, several measures should be taken in different fields, From optimizing of the existing energy systems to replacing them with renewable energy systems can be used to reduce GHGs.

Cacciali L *et al*. (2023) [2] investigated the multi-array design for hydrokinetic turbines in hydropower canals. In this study, they integrated a one dimensional channel model with a double multiple streamtube code and wake sub-models to determine an array layout for maximum array power. The results of the sensitivity analysis show that this design improved power conversion with closely spaced turbines and largely spaced arrays. As a result, it allows for a partial recovery of the total head variation for a new array deployed upstream. The results show that power output linearly scales for the array numbers less than 6.

Niebuhr C. M. *et al*. (2019) [3] presented a review study on hydrokinetic turbines for canal installations. They discussed the limitations and advances and potentials of hydrokinetic turbines working with near-zero head. In the review, they paid special attention to the small scale-state of the art near-zero hydrokinetic technologies, to the knowledge gap, limitations of water-infrastructure

owners and operators, and economic analyses of the industry.

John B. *et al*. (2021) [4] presented a techno-economic analysis of a standalone micro-grid based on hydrokinetic turbine. The system was also equipped with battery bank to store electricity, and it was supposed to provide electricity for the villages near the rivers or canals. They also compared their proposed system with a hydrokinetic-PV-battery system, and concluded that the minimum cost of energy for their system is 11% less.

Supplying energy demands in rural areas is challenging because their energy demands must be provided through transmission grid and distribution networks that transmit electricity or natural gas from far away. Clean and renewable alternatives such as solar, wind, tidal, hydro, and geo-thermal energies can overcome the drawbacks of the fossil fuels, and omit the losses and expenses of electricity grids and gas pipeline networks.

According to the announcement of the Ministry of Energy in Iran, the number of dams in Iran reached 214 by 2021. These dams always use canals to transport water from one place to another mostly by using gravitational force and elevation difference only; hence, these canals have high a potential for hydrokinetic turbines and produce renewable electricity. The researchers have explored how to actualize this potential. For example, Schleicher *et al*. [5] designed a portable hydrokinetic turbine via the computational fluid dynamics (CFD) method. They created various blades, and investigated their performance, and their results revealed that a maximum power coefficient of 0.43 with a 73.7% efficiency relative to the Betz limit is reachable. Daskiran *et al*. [6] simulated the ventilation of a hydrokinetic turbine, and investigated the impact of aeration on turbine performance. They conclude that the turbine operates more stable when tip speed ratio (TSR) is higher. In another research, Rio *et al*. [7] numerically simulated the impacts of augmented diffuser on the performance of a hydrokinetic turbine. They realized that in a water current with the velocity of 1.5 m/s, maximum power coefficient for the turbine with and without diffuser is 0.487 and 0.285, respectively. In 2019, Attiya *et al*. [8] investigated a micro-hydrokinetic turbine that runs near the free surface. They studied the temporal and spatial features of the turbulent flow structure with large eddy simulation (LES) model. They demonstrated that the turbine efficiency is not susceptible to the free surface. Aguilar *et al*. [9] designed an appropriate multi-element hydrofoil for usage in a horizontal-axis hydrokinetic turbine. They utilized two dimensional CFD simulations and multi-objective optimization methods based on surrogate modeling. Their optimum multi-element design had a gap equal to 2.82% of the chord length (C1) and an overlap equal to 8.25% C1. Muratoglu and Yuce [10] designed a hydrokinetic turbine for river application via CFD simulation. The performance of the turbine in terms of torque, power, and thrust were tested, and the design was optimized. Their design was capable of producing 27 kW of power from a current with 2.7m/s velocity. Adnan *et al*. [11] designed and fabricate a horizontal axis turbine for low velocity flow of water. They implemented the SolidWorks software for modeling, ANSYS Fluent for CFD analyzing, and 3D printing for fabricating. They revealed that a rotor with a diameter of 0.6 m can generate approximately 150 W of power in a water current with velocity of 1.5 m/s. In another research work, the influence of a duct-augmented system on the overall performance of a straight-blade hydrokinetic turbine has been investigated by Tunio *et al*. [12]. Their proposed that duct was able to increase the hydropower production by double; however, the turbine experienced a higher stress in comparison to a bared turbine. Application of this turbine in low-velocity flow of Golden Gate Strait is studied by Mohammadi *et al*. [13]. In their investigation, they optimize the hydrofoil by coupling the Xfoil and particle swarm methods. As a result, hydropower production improved by 26% and 50% for currents with 0.5-2 m/s and 2-3 m/s velocity, respectively. Shashikumar and Madav [14] studied new V shape blades for hydrokinetic turbine both experimentally and numerically. Their novel design was capable to decrease the negative torque developed by the returning blade and the optimum power coefficient of equal to 0.42 was reported. Implementing an upstream deflector and its effects on the flow characteristics and startup performance of a hydrokinetic turbine is studied by Kang *et al*. [15]. They showed that adding deflector causes negative torque elimination and downstream vortices shrink and expand as the blades rotate. Nachtane *et al*. [16] designed and investigated the hydrodynamic performance of a hydrokinetic turbine with horizontal axis. Standard hydrofoil of NTSXX20 was utilized in their study, and they concluded that their tidal turbine can capture about 50 percent from TSR range 5-9.

Kumar *et al*. [17] showed that the impact of dams and their watersheds on different scales requires

an urgent policy on a global scale to deal with the emission of greenhouse gases from hydropower reservoirs. As a result, compared to dam-based hydropower technology, hydrokinetic technology is a suitable option for small-scale power generation such as household applications in off-grid power generation. Dhakal *et al*. [18] showed that gravity hydrokinetic turbines can be easily installed in existing water infrastructure with costs of 1021 to 1261 USD with a generator capacity of 1.6 kW. Tigabo *et al*. [19] investigated the possibility of hydrokinetic turbines usage in rural areas, where the grid is not available, from an economic perspective. This study was conducted in the Gomara River, upstream of the Blue Nile, Amhara region of Ethiopia. The energy demand of a representative household is selected for this study. In this study, the internal rate of return (IRR) was 17.4%, a payback period of 5.6 years, a present value of $4,826, and a total net present value of $89,764 were estimated. The findings showed that HKTs technology is economically and technically a suitable option for small-scale off-grid electrification. Mohammad Shaheswari Fard *et al*. [20] found that during operation, hydrokinetic turbines in the rivers and tides areas face changes in the flow direction that reduce their performance. Evaluation of hydrokinetic turbines in changeable conditions helps to estimate turbine performance, power stability, and power delivered to the grid. Water tunnel tests have been conducted with a 19.8 cm diameter horizontal axis model turbine, and showed performance degradation using three designs: no shroud, convergent-divergent shroud, and a diffuser shroud. The experimental results showed that the output power decreases in the off-axis currents for all of the designs. The reduction is initially negligible; however, it increases as the deflection angle increases. The convergent-divergent shroud experiences significantly less performance compared to the other two designs. Abutunis *et al*. [21] investigated the evaluation and performance improvement of multiple horizontal axis hydrokinetic turbines (HAHkTs) installed on one shaft. In this research work, the hydrodynamic performance of different configurations of single and multiple HAHkTs with carbon fiber polymer blades were evaluated in a water tunnel. Increasing the number of turbine rotors from one rotor to two rotors increased the efficiency by approximately 75% and reduced the operating TSR. The third rotor also increased the efficiency; however, the improvement was less due to the slower current passing through this rotor. A reducer duct was also installed, and its effect was studied. Finally, its effect on the performance of the multi-turbine system was investigated using a particle image velocimetry system. From the structural aspect, composite materials had more suitable properties than others.

Overall, implementing hydrokinetic turbine in local canals and rivers can distribute power generation all over the country. Distributed electricity generation at the place of consumption and places where there is no grid provides significant advantages such as eliminating network losses, reducing construction costs, and strengthening passive defense.

In the present study, hydraulic analysis of three cross-section profiles of existing water transfer canals from Gawshan dam is presented, and then hydrokinetic turbines are designed according to the hydraulic characteristics of the canals to generate renewable electricity. In these three canals (shown in Fig. 1), the water velocity for the canals a, b, and c is 0.9, 1, and 1.5 m/s, respectively. For these three paths, different hydrofoil profiles are evaluated, and for each canal, the geometric characteristics of the hydrofoil and its sections are extracted using the Schmitz's theory. Then by modeling the turbine rotor set in the SolidWorks software for each channel, the power that can be extracted from the water stream is calculated by modelling in the ANSYS Fluent. The present research work is focusing on low-flow velocities and designing hydrofoil blades with high efficiency that are capable to exploit energy from low-velocity flows. The results are validated with the existing hydrokinetic turbines available in the market and the economic, and environmental evaluation of the design are presented as well.

The main novelties of the present work include:

- Presenting a hydrokinetic turbine for power generation in low velocity streams in the rivers or canals.
- Evaluation of three different real canal shapes and sizes, which transfer water for agriculture and drinking purposes for about 20 km.
- Presenting free surface modeling and its impact on the power generation.
- Investigating of cavitation occurrence on the turbine blades.
- Proposing a correlation to estimate power generation by the turbine for different velocities.
- Combining XFOIL, with SolidWorks and ANSYS Fluent to solve the hydrodynamic problem.
- Presenting technical, environmental, and economic evaluations of the turbine rotor.

## 2. Problem definition

In the present research work, the feasibility of utilizing hydrokinetic turbine in water transfer canals, made of concrete for the Gawshan dam in Kurdistan province, Iran is investigated technically, economically, and environmentally. The twenty-kilometer canals, transfer water from the Gawshan dam, which is a clay core dam with 123 m height. Four access points are considered in four villages of Kechleh, Serbanaw, Haltoshan, and Tuankesh on the canal route. The water transferred from the tunnel reaches a large pond in Kamyaran. At the pond, by means of three trapezoidal concrete channels (Figure 1) water is transferred to the following destinations:

a) from the west side to the farmlands of the Elk route,

b) from the east side to the farmlands of Bilewar region, and

c) through Razavar river goes to a treatment plant and pumping station, where the water is purified and pumped to the city of Kermanshah to supply drinking water.

d) These channels are open channels, and the simulation has been done in two phases, water, and air. Also the floor and walls of the channels are made of concrete.

Hydraulic characteristics of the aforementioned canals is as table 1.

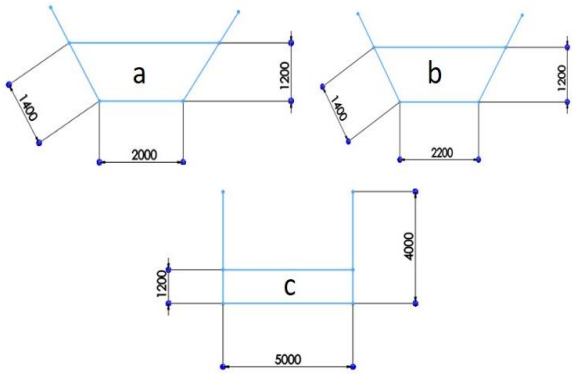


**Figure 1. Schematic representation of concrete water channels and water height in them: a) Elk path b) Bilewar path c) Razavar path.**

In Table 1, velocity (v), angular velocity (ω), rotational velocity (N), potential power of water ($P_{water}$), Reynolds number ($Re = \rho v D_h/\mu$), Froude number ($Fr = v/\sqrt{yg}$), specific velocity ($N_s = N\sqrt{Q}/H^{3/4}$), and specific diameter ($D_s = DH^{0.25}/\sqrt{Q}$) are reported. Turbine diameter (D) is 1 m, and water velocity for canals a, b, and c are 0.9, 1 and 1.5 m/s, respectively. y is the canal depth.

**Table 1. Hydraulic features for the studied water channels.**

| | $\omega$ $\left(\frac{rad}{s}\right)$ | N $(rpm)$ | $P_{water}$ (W) | $Re$ $\times 10^6$ | Fr | $N_s$ | $D_s$ |
|---|---|---|---|---|---|---|---|
| a | 9 | 86 | 285.5 | 2.47 | 0.26 | 789 | 0.54 |
| b | 10 | 95.5 | 391.7 | 2.7 | 0.29 | 789 | 0.54 |
| c | 15 | 143.3 | 1322 | 4.86 | 0.44 | 789 | 0.54 |

in which, $D_h$ is the hydraulic diameter of the canal, $Q$ is the volume flow rate from the swept area of the turbine, and head (H) is calculated according to the flow velocity by using the spouting equation $v = \sqrt{2gH}$.

According to the results presented in this table, the flow in the canal is subcritical ($Fr < 1$) and no hydraulic jump occurs. In addition, the flow is turbulent since the $Re > 2500$, consistent with the specific velocity/specific diameter ($N_s$-$D_s$) chart for turbines [22] and the calculations in Table 1, the most suitable turbine for all the canals is hydrokinetic turbine. Hence, in the following the designing steps of a hydrokinetic turbine, which is followed in the present research work, is explained.

## 3. Design of turbine

There are several differences between an airfoil used in aerospace engineering and an airfoil of a tidal turbine blade. For example, a tidal turbine blade is installed in water, where maintenance of the blades is problematic. In addition, because various loads are structurally imposed on the hub part, the wing tip must have a gradually thick shape. The characteristics of a tidal current power turbine are very similar to those of a wind turbine. While a tidal current power turbine uses a similar airfoil to that used in wind power, there is a significant difference between the viscosity and density of air and water; test and verification of the characteristics of an airfoil in seawater are therefore required. In the present research work, NACA4412 airfoil is used (Fig. 2), which is a common choice for the hydrokinetic turbines [23]. A reason for this selection lays in the fact that this airfoil is less sensitive to the surface roughness. Surface roughness is usually used for cavitation suppression on the hydrofoils. This is an important feature since it can reduce maintenance cost of the blades, where the current is not very clean.

The power generated by the turbine can be estimated according to below [24]:

$$\mathbf{P(W) = T.\omega} \quad (1)$$

in which, $T$ and ω are torque and angular velocity, respectively. The maximum generated power can

be estimated according to the Betz limit as equation (2).

$$\mathbf{P_{max}} = \frac{\mathbf{1}}{\mathbf{2}}\mathbf{c_{p.Betz}}\,\boldsymbol{\rho}\mathbf{v^3A} \quad (2)$$

In this equation, $v$ is the average velocity of inlet flow to the turbine, $A$ is the swept area of the turbine, and $c_{p.Betz}$ is the maximum power coefficient.

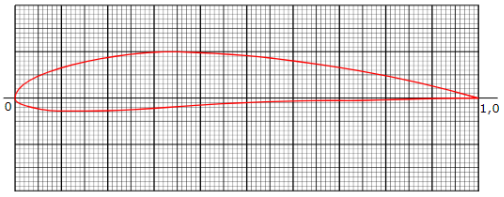


**Figure 2. Schematic representation of the NACA4412 Airfoil shape.**

### 3.1. Geometry design of blades

To design the geometry of the turbine's blade, the distribution of the chord length and twist angle at different points should be calculated. For this purpose, the Schmitz's theory [23] is used for the twist angle as follow.

$$\boldsymbol{\beta}(\mathbf{r}) = \frac{\mathbf{2}}{\mathbf{3}}\mathbf{arctan}\frac{\mathbf{R}}{\mathbf{rX}} - \boldsymbol{\alpha_D} \quad (3)$$

In equation (3), R is turbine radius, X is the TSR, r is the variable radius of a blade, and $a_D$ is the angle of attack that can be derived from the XFOIL software. Additionally, for distributed chord length equation (4) can be utilized.

$$\mathbf{c}(\mathbf{r}) = \frac{\mathbf{1}}{\mathbf{B}}\frac{\mathbf{16\pi r}}{\mathbf{C_L}}\mathbf{sin^2}\left(\frac{\mathbf{1}}{\mathbf{3}}\mathbf{arctan}\left(\frac{\mathbf{R}}{\mathbf{Xr}}\right)\right) \quad (4)$$

In this equation, $C_L$ is the lift coefficient that is calculated by the XFOIL software.

Because of the same lift coefficient and attack angle and also considering that the turbines of all three routes have 1-meter diameter, unique design and geometry is proposed. Figure 3 shows the geometry of the turbine that is designed in SolidWorks by considering the distributed chord length and twist angle.

**Figure 3. 3D model of the proposed turbine rotor modeled in SolidWorks.**

### 3.2. Hydrodynamic simulation

In order to solve the flow field around the turbine and their interaction, the simulation domains that follow the shape of the canals are depicted in figure 4.

Boundary conditions applied on different surfaces include:

- Velocity condition for the inlet surface
- Pressure boundary condition for the outlet surface.
- No-slip condition for the side-walls and surface of turbine's blades.
- Free surface condition in contact with the air for the top surface.

And the main assumptions include:

The flow is unsteady, incompressible, and isothermal. According to the Reynolds number, the flow is turbulent. Physical properties of flow such as density and viscosity are constant. The effect of gravity is taken into account. The turbine blades are completely submerged in water. According to the calculated Froude number which is less than 1, the flow is sub-critical.

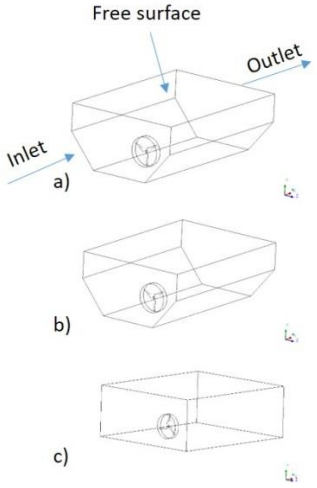


**Figure 4. The flow field domain for three paths: a) Elk path b) Bilewar path c) Razavar path.**

By applying the boundary conditions and assumptions to the models presented in figure 3 and 4, the flow field is discretized for solution as presented in figure 5.

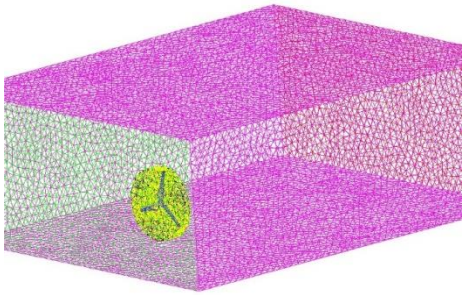

**Figure 5a. Generated tetrahedral mesh for flow field.**

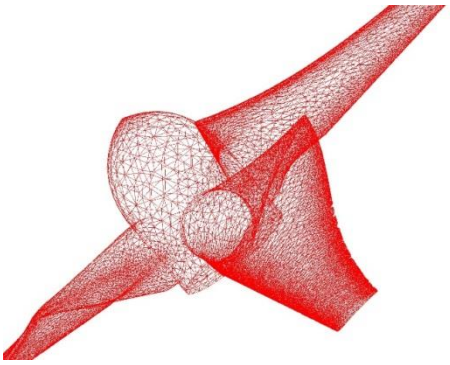

**Figure 5b. Generated tetrahedral mesh for the turbine.**

Governing equations on the model include mass conservation and the Navier-Stokes equation [21] that are summarized in Eqs. **Error! Reference source not found.** and **Error! Reference source not found.** as follow:

$$\frac{\partial u_i}{\partial x_i} = 0 \tag{5}$$

$$\rho\left(\frac{\partial u_i}{\partial t} + \frac{\partial\left(u_i u_j\right)}{\partial x_j}\right) = -\frac{\partial p}{\partial x_i} + \frac{\partial}{\partial x_i}\left[\mu\left(\frac{\partial u_i}{\partial x_j}\right)\right] \tag{6}$$

In these equations, ρ, μ, $u_i$, and P are density, dynamic viscosity, velocity components in the Cartesian coordinate system, and pressure, respectively. To solve the governing equations, transient flow with a time step of 0.01 second is used in the simulation of the fluid flow around the turbine. Also standard k-ε model has been used to consider the turbulence. The free surface simulation is done by considering the volume of fluid (VOF) model as below:

In the VOF method, the sharp interface between the two phases (e.g. liquid and gas) is determined using the VOF function, C, that represents the volume fraction of the reference phase in each computational cell, e.g. C = 0 in the gas, and C = 1 in the liquid ($0 \leq C \leq 1$) [25].

The evolution of the m-th fluid in a system on n fluids is governed by the transport equation:

$$\frac{\partial C_m}{\partial t} + \mathbf{V}.\nabla C_m = 0 \tag{7}$$

with the following constraint:

$$\sum_{m=1}^{n} C_m = 1 \tag{8}$$

i.e. the volume of the fluids is constant. For each cell, properties such as density $\rho$ are calculated by a volume fraction average of all fluids in the cell

$$\rho = \sum_{m=1}^{n} \rho_m C_m \tag{9}$$

The flowchart of the modeling and solving procedure is shown in figure 6.

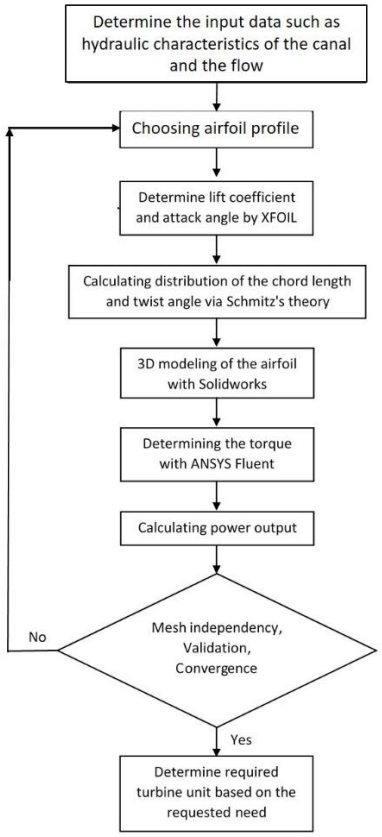


**Figure 6. Flowchart of modeling procedure.**

As the flowchart shows, the simulation would be confirmed if mesh independency, convergence of torque, and power output validation are done; otherwise, the simulation starts with new inputs data and new mesh if required. The volume of fluid (VOF) method is used to simulate the open channel, which is explained below:

### 3.3. Economic and environmental modeling

After determining the hydrodynamic feasibility of the turbine, its economic potential would be examined to find out if the proposed turbine is worth investing in or not. For this purpose, the net present value (NPV), and payback period (PB) of the turbine are calculated. The original investment cost is an important factor in calculating the NPV and PB. Economic analysis can be a helping hand tool for customers such as householders, energy service firms, and energy suppliers to secure their investment. The primary criterion for evaluating the economic analysis is the payback period (PB), which can be determined by the following equation [26]:

$$PB = \frac{I}{CF} \tag{10}$$

In this equation, the total initial investment of the components and net annual cash flow is represented by I and CF, respectively. The annual net cash flow of the project can be evaluated as follow:

$$\mathbf{CF = er - ex} \tag{11}$$

where *er* is income or positive cash flow, and *ex* is an expense or negative cash flow during one year. The net present value of the project (NPV), which is calculated during the lifespan of the project, indicates the added value created during the entire lifespan of the project. This value must be positive. A negative NPV means that the project is not beneficial.

$$\mathbf{NPV = S + \sum_{y=1}^{n} \frac{CF_y}{(1+r)^y} - I} \tag{12}$$

In this regard, n is the lifespan of the project, y is the counter, and r is the inflation rate, which is considered 5% for this project. The salvage value (S) of the project is neglected to make the evaluations more conservative.

Considering that the production of renewable electricity will reduce the fossil fuel consumption, therefore, this will also reduce the production of greenhouse gases. To calculate the emission reduction, the carbon dioxide emission coefficient of the national network is usually used. The value of this coefficient for the power grid is about 0.7 tons of carbon dioxide per megawatt hour. In addition, the carbon reduction income is about 10 dollars per ton of carbon dioxide reduction [27].

## 4. Results and discussion

To make sure about the results, the grid independency for the simulation analysis, validation of the output power for existing flow velocities with the available turbines in the market, and finally, convergence of the torque is presented. After these three steps, the results are presented and discussed in more details.

### 4.1. Grid independency

Due to boundary layer effect and also the geometrical complexity of the canals, the mesh size must be smaller near the boundaries and corners. But how small the mesh size and how many mesh elements should be used to solve the problem without losing accuracy or increasing run time of the model? For this purpose, grid independence study was done by considering coarse, medium, and fine meshes with 1,500,000, 2,920,000, and 7,410,000 tetrahedral elements. The grid resolution was checked by the generated power. Generated power for these three grid sizes are 550, 536, and 525.75 W.

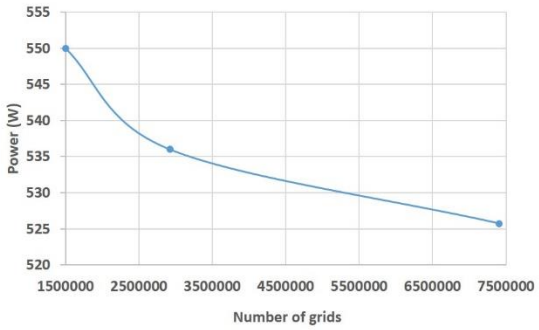


**Figure 7. Power curve based on the number of different meshes.**

Due to the fact that the difference between generated power for medium and fine mesh is less than 2%, the model with the medium mesh is adopted for the simulation.

### 4.2. Validation

A free stream hydrokinetic turbine with rotor diameter of 1 meter from smart hydro turbine company [28] is considered for the validation purpose. The specifications of this turbine and also the simulation are reported in table 2. The generated power reported in the catalog of the company and the results of the present simulation are compared for velocities from 0.9 m/s to 3.5 m/s. As shown in figure 8, these results are in good agreement.

**Table 2. Smart free stream turbine and the present simulation specifications.**

| Parameters (unit) | Manufacturer Data [28] | Present work |
|---|---|---|
| Output power (W) | 250-5000 | 117.45-6797 |
| Velocity range (m/s) | 1-3.1 | 0.9-3.5 |
| Rotational velocity range (rpm) | 90-230 | 85-335 |
| Number of blades | 3 | 3 |
| Rotor diameter (mm) | 1000 | 1000 |
| Min canal/river depth (m) | 1.1 | 1.2 |
| Min canal/river width (m) | 1.2 | 2 |

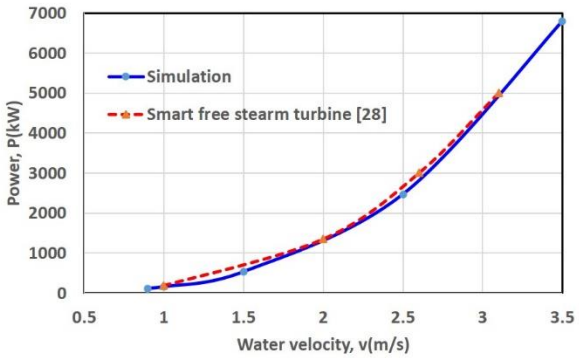


**Figure 8. Validation of the peresent study (simulation) with experimental data [28].**

### 4.3. Convergence

The torque generated by the rotor. which is the most important output, is selected as the convergence index. All parameters including velocity and pressure are effective in the torque calculation; therefore, the convergence of this parameter is of great importance to make sure about the model. Figure 9 shows the torque of the rotor for the Razavar path canal that is converged to 35.7 N.m after 2 seconds. The reason for the negative torque in the vertical axis is that the rotor rotates in the opposite direction. The output torque from the turbine initially varies widely up to 1.2 seconds. After that, there will be no significant changes. Therefore, solving the domain for 2 seconds is adequate and continuing the simulation can increase the computational cost with no significant benefit.

The results of the simulations and discussions are presented in the following.

The hydrodynamic force exerting on the turbine's blades is divided into the drag, lift, and radial forces. Drag acts on the blade in the flow direction, lift is perpendicular to the flow direction and exerts on the blade and radial force acts along the blade from the hub center to the blade tip. Drag is created due to blade resistance against fluid flow and comprises of pressure drag and friction drag. The radial force is due to asymmetric axial flow in the radial direction. The lift force is created as a result of the pressure difference between the two sides of the turbine blade, and causes the turbine rotation.

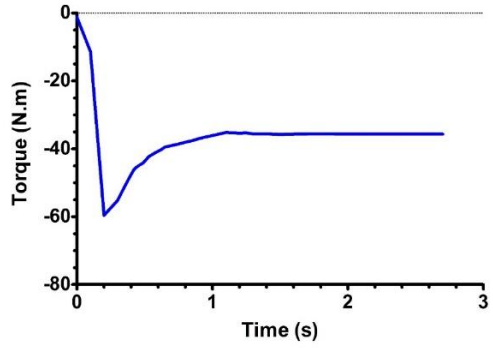


**Figure 9. Convergence of the torque for the Razavar path canal.**

The reason for this pressure difference is that when the fluid hits the airfoil at the edge of attack, the fluid velocity reaches zero, which is called the stagnation point. At this point, the velocity is zero, and according to the Bernoulli's law [29], the pressure will be maximum (Figure 10). Figure 10 is a cross-section of the blade and pressure distribution calculated by the ANSYS Fluent around it.

As water moves from the leading edge to the top of the airfoil, the velocity increases and the pressure decreases until it reaches the trailing edge of the airfoil, where the velocity has the highest value and the pressure has the lowest value [30]. The angle of attack for NACA4412 airfoil using XFOIL software is considered to be 9°, increasing this angle will cause flow separation and reducing lift force.

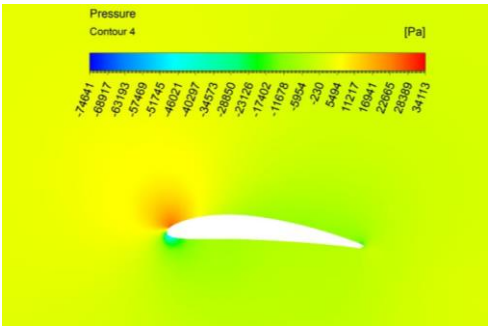


**Figure 10. Blade pressure distributions for Razavar path.**

The distribution of the gauge pressure on the turbine blades are shown for the three canals in Figure 11. According to this figure, the maximum gauge pressure for the three canals in Elk, Bilewar and Razavar are 16580 Pa, 18662 Pa, and 34113 Pa, respectively. The difference in the pressure distribution is due to the different flow velocity inlet.

The minimum gauge pressure for the three paths of Elk, Bilewar and Razavar are -23127 Pa, -30098 Pa, and -74641 Pa. This pressure difference on the blade surface is used to create rotation in the turbine rotor. One may concern about the cavitation, the water temperature in the canals and rivers is mostly less than 20 ℃ and the vapor pressure at this temperature is $P_{vapor} = 2339$ Pa, while the minimum absolute pressure in the flow field for the three paths are $P_{abs,Elk} = 101325 - 23127 = 78198\, Pa$, $P_{abs,Bilewar} = 101325 - 30098 = 71227\, Pa$ and $P_{abs,Razavar} = 101325 - 74641 = 26684\, Pa$ since in all of the paths $P_{abs} \geq P_{vapor}$, therefore there will be no cavitation problem on the turbine blades.

Velocity contour of the turbine for the three canals is presented in

Figure. The velocity of fluid entering the turbine in these three canals of Elk, Bilewar, and Razavar is 0.9 m/s, 1 m/s, and 1.5 m/s, respectively. The tip speed, which is the maximum velocity for the three paths, is 4.5 m/s, 5 m/s, and 7.5 m/s. Since the tip velocity is equal to $V_{tip} = \omega r$, and the radius is 0.5 m, therefore, the angular velocity for the three paths would be 9 rad/s, 10 rad/s, and 15 rad/s, which they correspond to rotational velocity

of 85.94 rpm, 95.49 rpm, and 143.24 rpm, respectively. In addition, the $TSR = V_{tip}/V_{flow}$ of the rotor would be 5 for all the three paths.

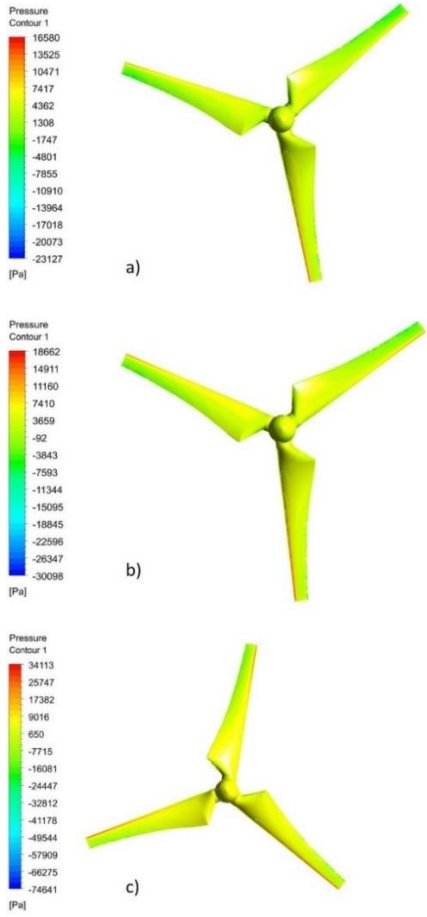


**Figure 11. Pressure distribution on the turbine blades for a) Elk path b) Bilewar path c) Razavar path.**

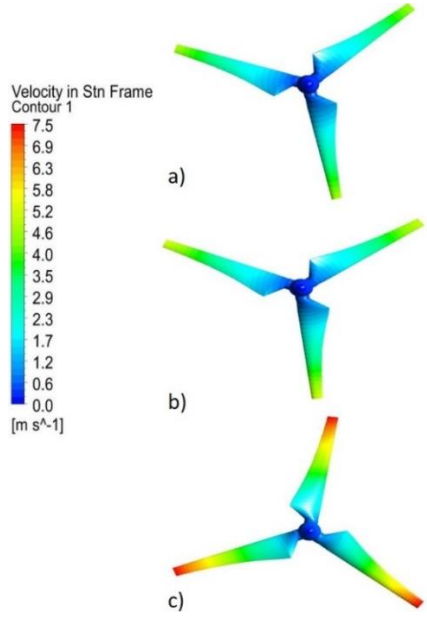


**Figure 12. Velocity contour of the turbine blade for a) Elk path b) Bilewar path c) Razavar path.**

Figure 13 shows air volume fraction and also the water free surface and atmospheric air interaction as the water flows over the turbine. As it is clear, water expands as it moves over the turbine; therefore, a wave forms and water level goes up due to the Bernoulli effect (velocity reduction, and mass conservation principal), as the water approaches the trailing edge of the blades its velocity increases and water level goes down for a short distance. After that when the turbine effect disappears, the water level returns to its initial level.

Figure 14 shows the velocity and pressure along the turbine axis from the upstream to the downstream, and the velocity contour along the Razavar canal (c), which shows that the velocity difference in the front and back of the turbine shows that this velocity difference causes pressure differences on both sides of the turbine and causes the lift force to rotate the turbine. As the fluid passes through the turbine, the flow returns to normal after a while.

By considering the power coefficient equal to $C_p = 0.45$ and blade radius equal to 0.5 meter, the turbine efficiency will be 90%. With the aforementioned characteristics, variation of the power output of the turbine with current velocity, which was shown in Figure 8, with the following correlation can be derived for the power generated by the turbine and water velocity range from 0.9 m/s to 3.5 m/s.

$$\mathbf{P(W) = 160.18\, V^{2.9889}} \quad (13)$$

The angle of attack ($\theta$), angular velocity $\omega$ ($rad/s$), TSR, momentum (N.m), are reported for the power (kWh/year), and efficiency three canals are reported in table 3 for turbine diameter of 1 m and canals' water velocity.

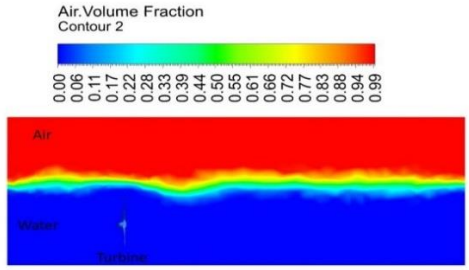


**Figure 13. Air volume fraction of the Razavar canal.**

**Table 3. Simulation results for the investigated canals.**

| | $\theta$ | $\omega$ | TSR | $C_p$ | M | P | $\eta$(%) |
|---|---|---|---|---|---|---|---|
| **a** | 9° | 9 | 5 | 0.45 | 13.05 | 1029 | 90 |
| **b** | 9° | 10 | 5 | 0.45 | 16 | 1401 | 90 |
| **c** | 9° | 15 | 5 | 0.45 | 35.7 | 4695 | 90 |

Another important parameter that is studied in this research work is the effect of free surface on power generation. According to the simulations that were also carried out without considering the free surface, while the blades are under water, the free surface has no impact on the power generation of the turbine.

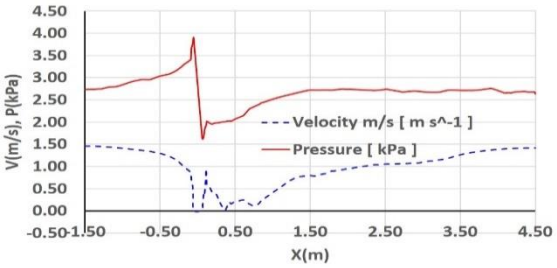


**Figure 14. Velocity contour of the canal c.**

### 4.4. Economic and environmental advantages

Economic evaluations are conducted for net present value (NPV) and payback period (PB) based on average global prices. In a conservative manner, the lifespan of these turbines is assumed to be 25 years despite the fact that the average lifespan of the hydropower plants is generally more than 40 years. The incomes include the sale of electricity, 0.173 $/kWh, and the reduction of carbon dioxide, 10 $/ton. To calculate the emission reduction, the carbon dioxide emission coefficient of the public electricity network is used that is 0.7 tons of carbon dioxide per megawatt hour of electricity. Additionally, based on the information of the manufacturers, the initial investment cost of the hydrokinetic turbine is 4500 ($/kW), and its maintenance cost is about 1.5% to 6% of its initial investment cost. According to the given data, the economic and environmental results of the project are calculated, and presented in table 4 for the three canals. In this table, ES ($/year), ACR (ton), and IOM($/year) are the annual electricity sale income, net annual income, annual $CO_2$ reduction, and operation and maintenance costs. The results show that the investment would be paid back in 3.1 years, and Razavar canal has the highest NPV due to higher water velocity. In addition, Razavars' canal is able to save 0.57 ton of carbon dioxide per year, which is the highest among the three canals.

**Table 4. Economic and environmental benefits of the project for different canals.**

| | ES ($) | ACR (ton) | CF ($) | I ($) | IOM ($\frac{\$}{year}$) | PB (year) | NPV ($) |
|---|---|---|---|---|---|---|---|
| **a** | 178.07 | 0.125 | 1.25 | 562.5 | 26.3 | 3.1 | 4738 |
| **b** | 242.5 | 0.17 | 1.7 | 720 | 36 | 3.1 | 6493 |
| **c** | 812.3 | 0.57 | 5.7 | 2412 | 120.6 | 3.1 | 21753 |

## 5. Conclusion

The main purpose of this research work was to design a hydrokinetic turbine for three exit canals of the Gawshan dam located in Kamyaran, Kurdistan, Iran. The main feature of these canals is their low-water velocities of 0.9, 1, and 1.5 m/s. Hence, the design of the turbines was constrained to this characteristic. In this regard, a standard profile was selected for the turbine, and different models were designed and hydrodynamically simulated using the Schmitz's theory and simulation in the SolidWorks, and ANSYS Fluent. After validation of the results with the existing turbine in the market, the model was subjected to technical, economic, and environmental evaluation. In summary, it can be concluded that:

Installing hydrokinetic turbines even in such low-water velocity canals is beneficial from the economic point of view and its PB is about 3 years for a lifespan of 25 years.

Since the lifespan of hydro turbines is usually more than 25 years, and can reach even 40 years, the economic benefits of the project would be even more.

The free surface has no impact on the magnitude of power generation by the turbine.

The proposed hydrokinetic turbine can reduce carbon dioxide production due to producing renewable electricity. The $CO_2$ reduction for Razavar, Bilewar, and Elk canals are 0.57, 0.17, and 0.125 tons/year, respectively. It is clear that installing multiple units of these turbines in several places can increase the pollution reduction.

The designed turbines can provide electricity for the rural areas with available water currents without needing the electricity from the public grid.

The excess electricity during the low load time can be used for hydrogen generation in a polymer electrolyte electrolyzer (PEL) and reconverting it to electricity in a polymer exchange membrane fuel cell (PEMFC) later during the high load time. The authors have started investigating this scenario as well.

Cavitation does not happen in the turbine.

## 5. References

[1] Net Zero Coalition | United Nations.

[2] Cacciali L, Battisti L, Dell'Anna S. Multi-Array Design for Hydrokinetic Turbines in Hydropower Canals. Energies. 2023; 16(5):2279. https://doi.org/10.3390/en16052279.

[3] Niebuhr C. M., Van Dijk M., Neary V. S., and J. N. Bhagwan, A Review of Hydrokinetic Turbines and Enhancement Techniques for Canal Installations:

Technology, Applicability and Potential, Renewable and Sustainable Energy Reviews, Volume 113, 2019, 109240, https://doi.org/10.1016/j.rser.2019.06.047.

[4] John B., Varghese J., Sizing, and Techno-Economic Analysis of Hydrokinetic Turbine-based Standalone Hybrid Energy Systems, Energy, Volume 221, 2021, 119717, https://doi.org/10.1016/j.energy.2020.119717.

[5] Schleicher WC, Riglin JD, and Oztekin A. Numerical characterization of a preliminary portable micro-hydrokinetic turbine rotor design. Renew Energy [Internet]. 2015 Apr;76:234–41. Available from: https://linkinghub.elsevier.com/retrieve/pii/S0960148114007472.

[6] Daskiran C, Attiya B, Riglin J, and Oztekin A. Large eddy simulations of ventilated micro hydrokinetic turbine at design and off-design operating conditions. Ocean Eng [Internet]. 2018 Dec;169:1–18. Available from: https://linkinghub.elsevier.com/retrieve/pii/S0029801818317190.

[7] Rio JS Del, Mancilla C, Hincapié-Zuluaga D, and Chica E. A numerical simulation of horizontal axis hydrokinetic turbine with and without augmented diffuser. Int J Renew Energy Res. 2018 Dec;8(4):1833–9.

[8] Attiya B, Altimemy M, Daskiran C, Liu I-H, and Oztekin A. Micro-Hydrokinetic Turbine Operating in the Vicinity of a Free Surface: Multiphase Large Eddy Simulations [Internet]. 2019. Available from: https://doi.org/10.1115/IMECE2019-10899.

[9] Aguilar J, Rubio-Clemente A, Velasquez L, and Chica E. Design and Optimization of a Multi-Element Hydrofoil for a Horizontal-Axis Hydrokinetic Turbine. Vol. 12, Energies . 2019.

[10] Muratoglu A and Yuce MI. Design of a River Hydrokinetic Turbine using Optimization and CFD Simulations. J Energy Eng [Internet]. 2017 Aug;143(4):4017009. Available from: https://ascelibrary.org/doi/10.1061/%28ASCE%29EY.1943-7897.0000438.

[11] Adnan M, Tahir MA, Jamal MA, Aslam Z, Irfan T, and Umer M. Design, Analysis, and Fabrication of Water Turbine for Slow-Moving Water. J Energy Resour Technol [Internet]. 2022 Aug;144(8). Available from: https://asmedigitalcollection.asme.org/energyresources/article/144/8/082102/1122253/Design-Analysis-and-Fabrication-of-Water-Turbine.

[12] Tunio IA, Shah MA, Hussain T, Harijan K, Mirjat NH, and Memon AH. Investigation of duct augmented system effect on the overall performance of straight blade Darrieus hydrokinetic turbine. Renew Energy [Internet]. 2020 Jun;153:143–54. Available from: https://linkinghub.elsevier.com/retrieve/pii/S0960148120301981.

[13] Mohammadi S, Hassanalian M, Arionfard H, and Bakhtiyarov S. Optimal design of hydrokinetic turbine for low-speed water flow in Golden Gate Strait. Renew Energy [Internet]. 2020 May;150:147–55. Available from: https://linkinghub.elsevier.com/retrieve/pii/S096014811932021X.

[14] C M S and Madav V. Numerical and experimental investigation of modified V-shaped turbine blades for hydrokinetic energy generation. Renew Energy [Internet]. 2021 Nov;177:1170–97. Available from: https://linkinghub.elsevier.com/retrieve/pii/S0960148121007680.

[15] Kang C, Zhao H, Zhang Y, and Ding K. Effects of upstream deflector on flow characteristics and startup performance of a drag-type hydrokinetic rotor. Renew Energy [Internet]. 2021 Jul;172:290–303. Available from: https://linkinghub.elsevier.com/retrieve/pii/S0960148121003992.

[16] Nachtane M, Tarfaoui M, El Moumen A, Saifaoui D, and Benyahia H. Design and Hydrodynamic Performance of a Horizontal Axis Hydrokinetic Turbine. Int J Automot Mech Eng [Internet]. 2019 Jul;16(2):6453–69. Available from: https://172.16.102.60/ijame/article/view/62.

[17] Kumar A, Sharma MP, and Kumar A. Green house gas emissions from hydropower reservoirs: Policy and challenges. Int J Renew Energy Res. 2016;6(2).

[18] Dhakal R, Nepal A, Acharya A, Kumal B, Aryal T, Williamson SJ et al. Technical and economic prospects for the site implementation of a gravitational water vortex power plant in Nepal. In: 2016 IEEE International Conference on Renewable Energy Research and Applications, ICRERA 2016. 2017.

[19] Tigabu MT, Guta DD, and Admasu BT. Economics of Hydro-Kinetic Turbine for off-grid Application: A Case Study of Gumara River, Upper Blue Nile, Amhara, Ethiopia. Int J Renew Energy Res. 2019;9(3).

[20] Shahsavarifard M, Bibeau EL. Performance characteristics of shrouded horizontal axis hydrokinetic turbines in yawed conditions. Ocean Eng. 2020;197.

[21] Abutunis A, Taylor G, Fal M, and Chandrashekhara K. Experimental evaluation of coaxial horizontal axis hydrokinetic composite turbine system. Renew Energy. 2020;157.

[22] PE KEN. How to select turbomachinery for your application. Barber-Nichols Inc. 2020;

[23] Jo C hee, Yim J young, Lee K hee, Rho Y ho. Performance of horizontal axis tidal current turbine by blade configuration. Renew Energy [Internet]. 2012;42:195–206. Available from: http://dx.doi.org/10.1016/j.renene.2011.08.017

[24] Kazemi K, Ebrahimi M, Lahonian M, Babamiri A. Micro-scale heat and electricity generation by a hybrid solar collector-chimney, thermoelectric, and wind turbine. Sustain Energy Technol Assessments [Internet]. 2022 Oct;53:102394. Available from: https://linkinghub.elsevier.com/retrieve/pii/S2213138822004465.

[25] Baraldi A, Dodd MS, and Ferrante A. A mass-conserving volume-of-fluid method: Volume tracking and droplet surface-tension in incompressible isotropic turbulence. Comput Fluids [Internet]. 2014;96:322–37. Available from: http://dx.doi.org/10.1016/j.compfluid.2013.12.018.

[26] Babamiri A, Gharib M, and Ebrahimi M. Multi-criteria evaluation of a novel micro-trigeneration cycle based on α-type Stirling engine, organic Rankine cycle, and adsorption chiller. Energy Convers Manag [Internet]. 2022 Feb;253:115162. Available from: https://linkinghub.elsevier.com/retrieve/pii/S0196890421013388.

[27] Hope C, Newbery D. Calculating The Social Cost Of Carbon. Rev Lit Arts Am [Internet]. 2006;(October):24. Available from: http://www.electricitypolicy.org.uk/pubs/wp/eprg0720.pdf%5Cnhttp://login.ezproxy.library.ualberta.ca/login?url=http://search.ebscohost.com/login.aspx?direct=true&db=eoh&AN=0945762&site=ehost-live&scope=site.

[28] Monofloat S. Smart monofloat turbine. https://smart-hydro.de/ accessed on 1/1/2024

[29] Lin CE, Phan BC, and Chuang JS. Small wind generation using complex airfoil turbine. Cogent Eng. 2019;6(1).

[30] Sokołowski P, Czarnigowski J, Magryta P. CFD simulation study of air flow around the airfoil using the Magnus effect. Appl Comput Sci. 2015;11(3):19–33.